Growth, microstructure, UV and orange pink emission from ZnO nanocones

Santa Chawla *, K. Jayanthi, Sukhvir Singh, Harish Chander

National Physical Laboratory, New Delhi 110 012, India

ARTICLE INFO

ABSTRACT

ZnO nanocones are synthesized as freestanding powder as well as thin film by precipitation in a highly alkaline aqueous solution. X-ray diffraction demonstrated well-formed wurtzite crystal structure. The microstructure and morphology of individual nanocone were studied by transmission electron microscopy. Photoluminescence studies show strong UV emission in both powder and thin film form. Powder samples also show weak orange pink emission under UV excitation. High UV to visible emission ratio implies purity of the crystallites. However, the ZnO crystallites are also excitable by purple/blue light to emit in orange/red region and act as down conversion phosphor in the visible range indicating role of some intragap states. Fluorescence lifetime spectroscopy indicates fast recombination in hundreds of picoseconds range and complex charge transfer process in the microsecond range suggesting role of excitons and intragap states in the photophysical process.

© 2008 Elsevier B.V. All rights reserved.

1. Introduction

Recently, there have been extensive studies on optical properties of zinc oxide due to its size- and shape-dependent optical responses [1–3]. ZnO has been studied in different growth forms such as nanoneedles, nanowires, nanorods, flowers, tetrapods, etc. [4–8] for its luminescence properties. ZnO has a wide direct band gap of 3.37 eV which makes it promising for fabricating UV-emitting devices. Efficient excitonic emission at ambient temperature is possible due to large exciton binding energy of 60 meV which can be tuned up to 120 meV by controlling the active layers in ZnO quantum structures [9]. Preparation of nanosized ZnO has been carried out by different methods like pulsed laser deposition, molecular beam epitaxy, aerosol, micro-emulsion, sol–gel, atomic layer deposition, solid-state reaction, wet chemical synthesis and spray pyrolysis [10–18]. Thin films of ZnO with controlled thickness and conductivity can be fabricated by chemical deposition technique. Thin films of semiconductor nanoneedles and nanowires find application in fields requiring high surface area and pointed geometry, luminescence in general and field emission devices in particular. Conical crystal growth is expected to be very

effective for such devices. We report conical growth of ZnO nanocrystals by simple aqueous solution method both in thin film form as well as free standing powder and discuss their crystallinity, microstructure, luminescence characteristics and photophysical processes. The emission properties of ZnO polycrystalline aggregate as well as thin films are sensitive to growth conditions which are mostly responsible for inclusion of defects in the crystal.

2. Experimental details

ZnO was prepared by a wet chemical method using dilute (0.027 M) zinc acetate aqueous solution as a precursor [19]. A highly alkaline environment (pH~10) was created by adding ammonia solution and ultrasonification. On addition of NH_4OH, zinc hydroxide started precipitating. Well-cleaned fused quartz substrates were then introduced into the liquid to lie horizontally. The solution was covered and kept in a preheated oven at 90 °C for 18 h. The quartz substrates with deposited thin film of synthesized ZnO were taken out and cleaned with deionized water and alcohol repeatedly. The solution was decanted and ZnO powder settled in the bottom was repeatedly washed with deionized water and alcohol in ultrasonic bath. Cleaning was necessary to remove the surface impurities and minimize particle agglomeration. ZnO

* Corresponding author. Tel.: +91 11 45609242; fax: +91 11 25726938.
E-mail address: santa@mail.nplindia.ernet.in (S. Chawla).

powder was dried in an oven at 90 °C for 4 h. Deposited thin film was kept in an oven for few days at 90 °C. The chemical route for formation of ZnO particles in highly alkaline environment can be expressed as follows:

$$Zn(CH_3COO)_2 + NH_4OH \rightarrow Zn(NH_3)_4 \, (OH)_2$$
$$+ CH_3COOH \rightarrow Zn(OH)_2 + NH_4CH_3COO$$
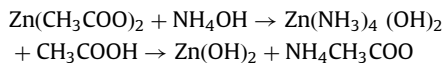
Upon heating, $Zn(OH)_2$ decomposes to form ZnO. In the reaction process, the formation of the amino complex $Zn(NH_3)_4^{2+}$ is dependent critically upon the alkalinity (pH) of the solution. By increasing pH of the solution with addition of more NH_4OH, more amino complex is formed and formation of ZnO would take place. The crystalline phase and average crystallite size of freestanding powder and thin film were characterized by powder X-ray diffraction (XRD) by using Brucker-AXS D8 Advance Diffractometer (with DIFFRAC plus software) using CuK_α (0.15408 nm) radiation. The crystallite shape and microstructural investigation of the ZnO powder particles has been carried out under transmission electron microscope (TEM) make JEM, model JEOL 200 Cx operated at accelerating voltage 160 kV. Room temperature photoluminescence (PL) measurements of the powder and thin film samples were carried out using Perkin Elmer LS55 fluorescence spectrometer with a Xe lamp source. Fluorescence lifetime spectroscopy was done at room temperature by measuring time-resolved decay of PL using time-correlated single-photon counting (TCSPS) technique with FLSP920 fluorescence lifetime spectrometer of Edinburgh Instruments, using a microsecond pulse Xe flash lamp and a nanosecond pulse hydrogen lamp.

3. Results and discussion

The synthesized ZnO powder and thin film look white under room light. However, under a UV lamp they glow in orange pink. XRD pattern of synthesized ZnO powder as shown in Fig. 1(a), suggested well formed pure hexagonal wurtzite phase as confirmed by Joint Committee on Powder Diffraction Standards (JCPDS) Card No. 36-1451. All the diffraction peaks were very well formed for the powder samples whereas thin film sample showed absence of any preferred orientation in good agreement with similar work [20]. The broadening of the diffraction peaks indicated small size of the crystallites with a longer dimension along c-axis manifested by a relatively sharper (0 0 2) peak for the
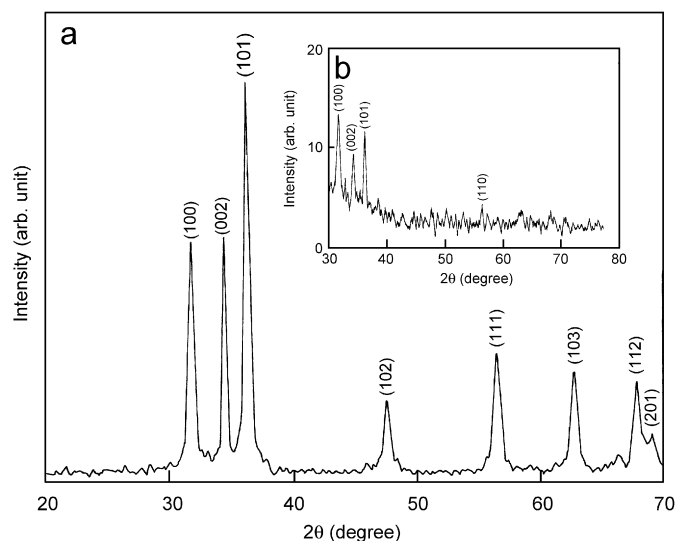
Fig. 1. XRD spectra of ZnO nanocrystals (a) powder (b) thin film deposited on quartz substrate showing formation of hexagonal phase.

powder samples. The average crystallite dimensions calculated by using Scherrer formula was 19 nm along a-axis and 30 nm along c-axis for the powder. The calculated average crystallite size was 19 nm along a-axis for thin film samples. The length of a- and c-axis was calculated to be 0.3257 and 0.5235 nm for the thin film sample. The length of a- and c-axis was 0.3246 and 0.5200 nm for the powder sample. The discrepancy in the interplanar spacing (d values) and lattice parameter, e.g., c-value in the free standing powder and film is due to residual stress in the films [20]. The strain on the c-axis is calculated as $\varepsilon = (c_{film} - c_{powder})/c_{powder} = 0.0067$ GPa. As film deposition and powder formation was done from the same solution, the growth conditions are exactly identical. The film stress parallel to the film surface has been calculated, by using a formula suitable for hexagonal lattice and using biaxial strain model [21], to be 1.5682 GPa. As the films were deposited on fused quartz substrate, residual stress on films parallel to the surface is high. Usually oriented growth is done on lattice-matched substrates, but as the residual stress is high for films on amorphous fused quartz slides oriented growth was not observed.

Microstructure as shown in TEM micrograph (Fig. 2a) clearly revealed presence of elongated conical particles. However, some needle-like particles are also seen in the micrograph. Average length of cone-shaped particles is about 235 nm and the length of the needle-like grains was calculated to be 350 nm. Selected area electron diffraction (SAED) pattern of the corresponding area was also recorded and shown as inset in Fig. 2(a). SAED pattern clearly indicated the polycrystalline nature of such grains. Electron diffraction pattern was carefully analyzed and it confirmed the formation of single-phase hexagonal ZnO structure. On indexing the SAED pattern, the $(h k l)$ planes (1 0 0), (1 0 1), (1 0 2), (1 1 0), (0 0 4) and (1 0 4) were identified (JCPDS Card No. 36-1451). Microstructure of these ZnO particles were also recorded at very high magnification (250,000 ×) which reveal inclusions of very fine round-shaped particles of average size 8 nm in some of the conical grains (Fig. 2b). Ratio of bottom to tip diameter of cone-shaped particles are 8:1. In the present case simple ZnO nanocones as well as complex conical overgrowth in stand-alone particles was observed.

One-dimensional nanostructure has attracted lot of attention for field emission devices due to their small device size, high efficiency. ZnO has a specific advantage due to low electron affinity and its shape can be tailored to have high aspect ratio. Field emission is mainly dependent on tip morphology as sharper and smaller the tip, lower will be the turn on voltage. The present ZnO nanocones prepared by a simple aqueous solution growth have very sharp tips of few nanometer diameter and such structures can be potentially used in field emission devices.

Photoluminescence excitation (PLE) and emission spectra of ZnO nanoparticles are shown in Fig. 3. ZnO in both powder and thin film form show an excitation peak at 242 nm. PL emission spectra show strong UV emission at 393 nm (3.15 eV) and much smaller visible (orange) emission. The UV emission showed Stoke's shift as the emitted energy is lower that the band gap energy of ZnO. In the thin film form, the intensity of UV emission improved considerably and visible emission was negligible when excited by 242 nm light. UV emission is due to band edge excitonic recombination and visible emission arises from defect levels in ZnO. The intensity ratio of UV (393 nm) to orange (595 nm) peak emission was calculated to be 14 for powder sample and 96 for thin film samples. The high-intensity ratio of band edge emission to defect level emission indicates very less number of point defects in the samples. Green emission in ZnO has been widely reported in the literature [22–25] and has been attributed to oxygen vacancy-related centre. Negligible green emission in our samples suggests very low concentration of oxygen vacancy in the

a

b
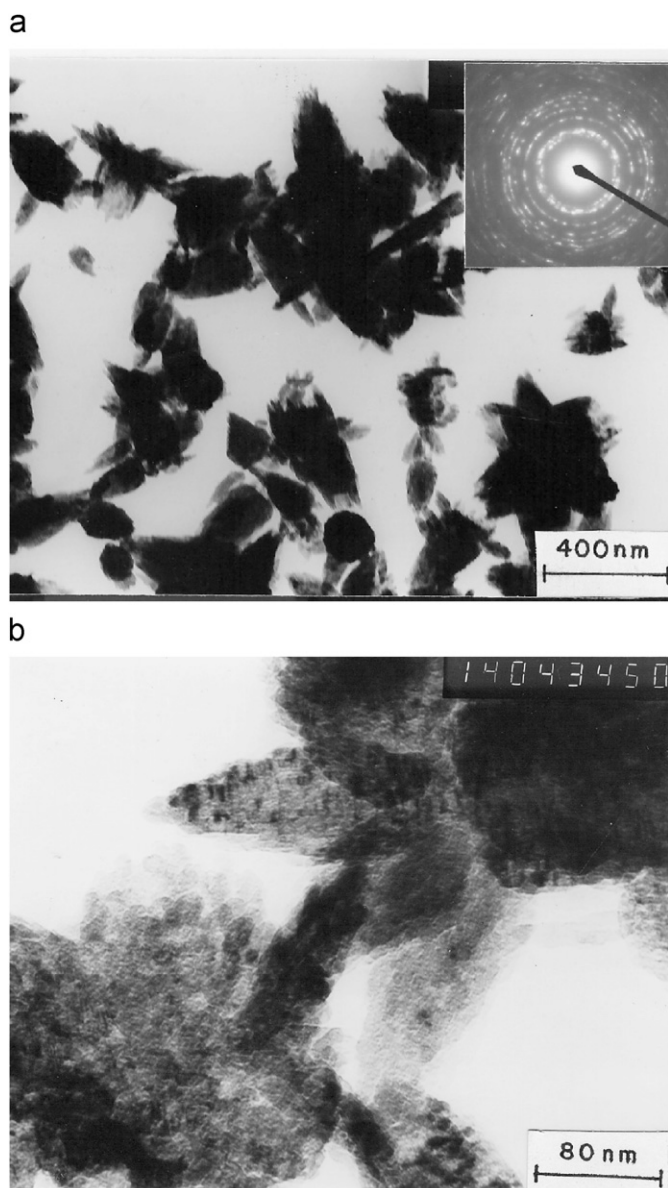
Fig. 2. TEM images of freestanding nanocrystals of ZnO in the powder form (a) inset shows SAED pattern, (b) highly magnified image shows conical overgrowth on cone-shaped particle as well as inclusion of small particles.

Fig. 3. (Colour online) PL excitation and emission spectra of ZnO powder and thin film. The emission spectra is taken at peak excitation wavelength 242 nm. The visible part of the emission is multiplied 10 times.
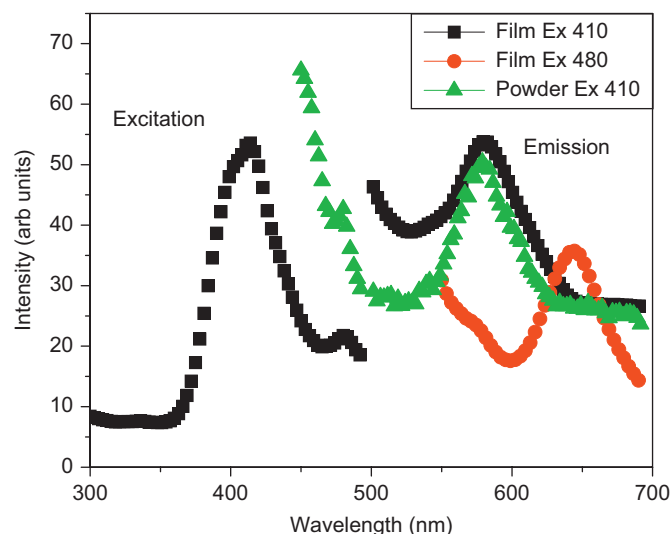
Fig. 4. (Colour online) PL excitation and emission spectra of ZnO powder and thin film showing the down conversion property in the visible region. The excitation spectra peaks at 410 and 480 nm and corresponding emission is in orange and red. The inset indicate the excitation wavelength for the respective emission spectra.

ZnO nanocones. Moreover, prolonged low-temperature (90 °C) annealing of ZnO film in air reduced the oxygen vacancy centres so that visible emission in green is negligible. The excitation spectra for the orange emission show additional peaks around 410 nm (3.02 eV) and 480 nm (2.58 eV) as shown in Fig. 4. It is encouraging to note in Fig. 4 that ZnO nanocrystals can be excited by purple/blue light to emit in orange and red. The excitation spectra of Fig. 4 cover the wavelength range of commercially available blue LEDs. Since ZnO can be produced in a cost-effective process, the possibility of using ZnO to make a phosphor-converted LED to produce white light can be a feasible application. Such property of ZnO has not been reported before.

Time-resolved PL decay measured for two emission wavelengths when excited by 242 nm light of μs pulse width is shown in Fig. 5(a). The decay curves (Fig. 5a) could be expressed mathematically as

$$R(t) = A + \sum_{i=1}^{n} B_i e^{-t/\tau i}$$

where τ_i represents characteristic lifetime and denotes the time taken to decay from the beginning of the decay to 37% of the original value, B_i is a pre-exponential factor, which includes both instrumental and sample parameters. In a multiexponential decay, Relative contribution ratio of individual components can be inferred from values of B_i. Exponential fitting of the decay curves yield luminescence lifetimes and the results are listed in Table 1.

The three-dimensional display of time-resolved emission spectra (TRES) is shown in Fig. 5(b) in which a family of decay curves are plotted as a function of emission wavelength. The lifetime contour map is shown in Fig. 5(c) which shows an overview of the complex decay pattern. The cursors indicate both a time-resolved emission spectrum and the corresponding decay kinetics simultaneously at a particular incidence. In Fig. 5(c), the cursors indicate that at 275 μs after the excitation, the near band

a

b

c
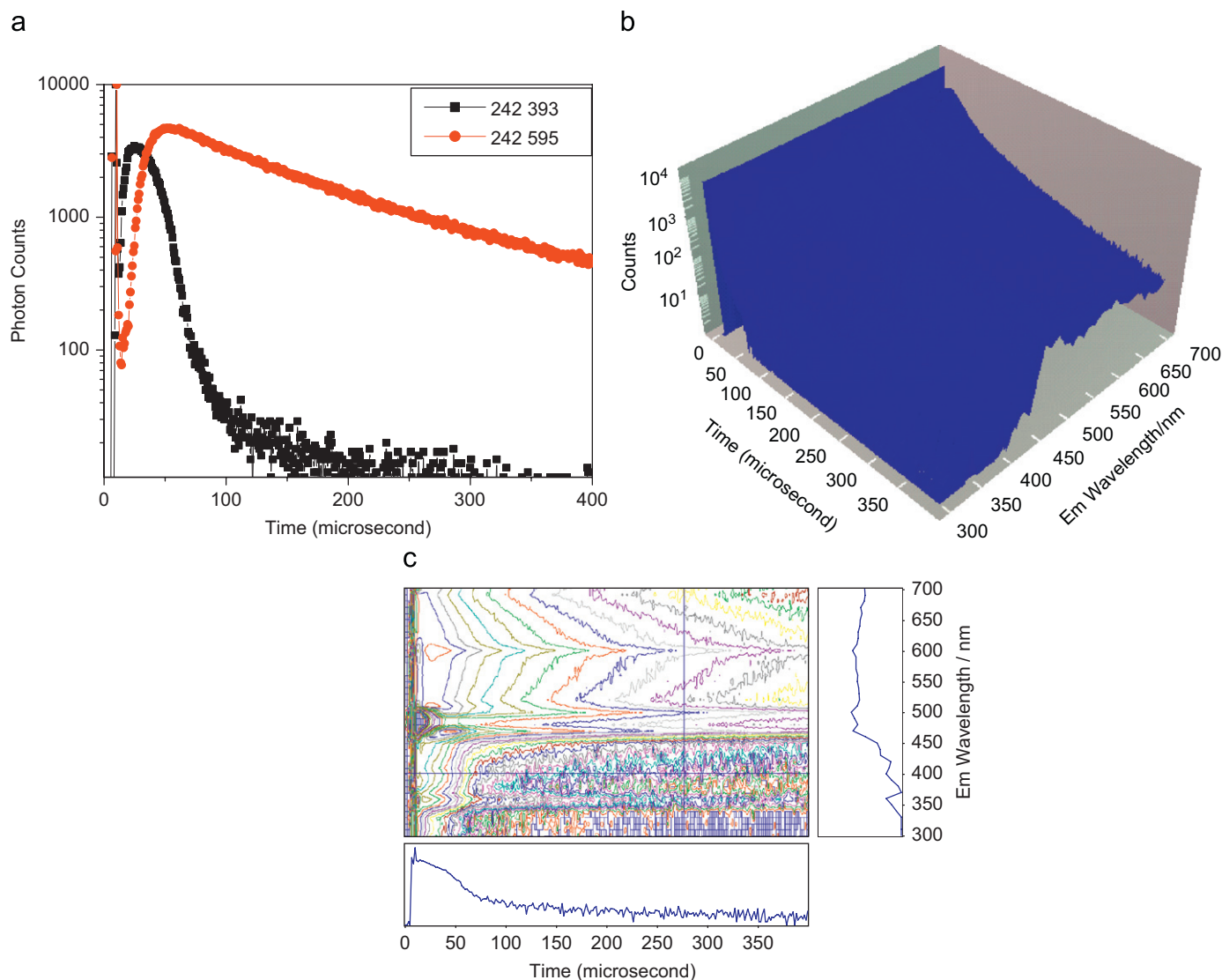
Fig. 5. (Colour online) (a) time-resolved decay of PL when excited by 242 nm light, the inset signifies excitation and emission wavelength, respectively, (b) 3D TRES-emission time map and (c)100 emission contour map of ZnO nanocones. The variation in decay characteristic between UV and visible (orange) emission is apparent.

Table 1

Emission wavelength (nm)	τ_1 (μs)	Relative contribution (%)	τ_2 (μs)	Relative contribution (%)
393	6.1	43	46.6	57
595	111	100		

edge UV emission has completely decayed whereas the visible emission still persists.

The decay of near band edge UV emission also has a component in the nanosecond range as observed by excitation with a nanosecond flash lamp. The observed single exponential decay gave a lifetime of 800 ps. The fast decay gets masked in the microsecond scale decay curve. The fast decay of UV emission suggests the role of excitonic recombination process.

UV emission in ZnO crystal is usually attributed to the near band edge emission due to radiative recombination of electron and holes in form of excitons. It is argued [23] that enhancement of UV emission could result from desorption of water which leads to reduction of nonradiative centres. Hydrogen doping can also passivate the visible emission while strongly enhancing the UV

emission. As the UV emission energy (3.15 eV) is less than band gap energy of ZnO, the UV emission may be arising from a donor-bound exciton [24]. The orange 595 nm (2.08 eV) emission possibly arises from recombination of trapped electrons from a shallow donor level (Zn_i) with holes trapped in oxygen interstitial (O_i) centre. The energy location of Zn_i and O_i level is reported to be below the conduction band by 0.22 eV [24] and 2.28 eV [25], respectively. This recombination can then explain the 2.08 eV orange emission. Due to large diameter of oxygen atom, probability of oxygen atoms being in the interstitial site is low and hence the intensity of the orange emission is less. Single exponential decay of 595 nm emission when excited by 242 nm light (Fig. 5a), supports the mechanism. The conductivity measurement of the thin film indicates it to be almost intrinsic. In the undoped ZnO the room temperature conductivity could only arise from point defects, which also give rise to visible luminescence. As negligible visible luminescence is observed in the ZnO films, the point defects are very few and the luminescence is dominated by near band edge UV emission. However, lower than band gap excitation ((3.02, 2.58 eV) suggest the role of some intragap states in the charge transfer process. Excitation of electrons can be from valence band to donor level Zn_i or between

donor–acceptor (DA) pair. Recombination of these electrons to different acceptor point defects/ surface states may give rise to the visible emission. Due to large surface area of the nanocones, surface states may form intragap states and can play a role in the emission process. The broad visible emission is probably associated with distant DA pairs which has long radiative lifetime [26]. This also account for the afterglow in 595 nm emission compared to the near band edge emission (Fig. 5a). As the number of intragap states is few, a random distribution of donor- and acceptor-type states can be assumed throughout the crystal.

4. Conclusions

Nanocones of ZnO as freestanding powder as well as thin film were synthesized by a simple aqueous solution method. Sharp pointed geometry of ZnO nanocones could be useful for field emission devices. Strong UV emission and negligible visible emission in ZnO nanocones indicate dominance of near band edge excitonic recombination compared to defect-related emission. However, orange/red emission in ZnO nanocrystals when excited by purple/blue light suggest the possibility of using ZnO as a down conversion phosphor in the visible with possible application in phosphor-converted LED for producing white light.

References

[1] L.E. Brus, J. Lumin. 70 (1996) 1.
[2] X. Peng, L. Manna, W. Yang, J. Wickham, E. Schar, A. Kadavanich, A.P. Alivisatos, Nature (London) 404 (2000) 59.
[3] J. Hu, L.S. Li, W. Yang, L. Manna, L.W. Wang, A.P. Alivisatos, Science 292 (2001) 2060.
[4] C.B. Murray, D.J. Norris, M.G. Bawendi, J. Am. Chem. Soc. 115 (1993) 8706.
[5] N. Nirmal, B.O. Dabbousi, M.G. Bawendi, J.I. Macklin, J.K. Trautman, T.D. Harris, L.E. Brus, Nature (London) 383 (1996) 802.
[6] S.A. Empedocles, D.J. Norris, M.G. Bawendi, Phys. Rev. Lett. 77 (1996) 3873.
[7] D. Matsuura, Y. Kanemitsu, T. Kushida, C.W. White, J.D. Budai, A. Meldrum, Appl. Phys. Lett. 77 (2000) 2289.
[8] A.L. Efros, M. Rosen, Phys. Rev. Lett. 78 (1997) 1110.
[9] H.D. Shun, T. Makino, Y. Segawa, M. Kawasaki, A. Ohtomo, K. Tamura, J. Appl. Phys. 91 (2002) 1993.
[10] M. Joseph, H. Tabata, T. Kawai, Appl. Phys. Lett. 74 (1999) 17.
[11] X. Wang, Y.M. Lu, D.Z. Shen, Z.Z. Zhang, B.H. Li, B. Yao, J.Y. Zhang, D.X. Zhao, X.W. Fan, J. Lumin. 122 (2007) 165.
[12] M. Singhai, V. Chhabra, P. Kang, D.O. Shah, Mater. Res. Bull. 32 (1997) 239.
[13] S. Hingorani, V. Pillai, P. Kumar, M.S. Multani, D.O. Shah, Mater. Res. Bull. 28 (1993) 1303.
[14] S. Bandyopadhyay, G.K. Paul, S.K. Sen, Sol. Enegy Mater. Sol. Cell 71 (2002) 1.
[15] Quanchang Li, Vageesh Kumar, Yan Li, Haitao Zhang, Tobin J. Marks, Robert P.H. Chang, Chem. Mater. 17 (2005) 1001.
[16] Niloy Chakraborty, Debabrata Basu, Werner Fischer, J. Eur. Ceram. Soc. 25 (2005) 11.
[17] H. Zhang, X.L. Du, Q. Luo, J.F. Jia, C.Z. Gu, Q.K. Xue, Thin Solid Films 515 (2007) 7.
[18] Tian-Quan Liu, Osamu Sakurai, Nobuyasu Mizutani, Masanori Kato, J. Mater. Sci. 21 (1986) 3698.
[19] H.Q. Le, S.J. Chua, Y.W. Koh, K.P. Loh, Z. Chen, C.V. Thompson, E.A. Fitzgerald, Appl. Phys. Lett. 87 (2005) 101908.
[20] T. Saeed, P.O. Brien, Thin Solid Film 271 (1995) 35.
[21] R. Hong, Jianda Shao, Hongbo He, Zhengxiu Fan, J. Crystal Growth 290 (2006) 334.
[22] By Jih-Jen Wu, Sai-Chang Liu, Adv. Mater. 14 (2002) 215.
[23] R. Xie, T. Sekiguchi, T. Ishigaki, N. Ohashi, D. Li, D. Yang, B. Liu, Y. Bando, Appl. Phys. Lett. 88 (2006) 134103.
[24] B. Cao, W. Cai, H. Zeng, Appl. Phys. Lett. 88 (2006) 161101.
[25] B. Lin, Z. Fu, Y. Jia, Appl. Phy. Lett. 79 (2001) 943.
[26] D.G. Thomas, J.J. Hopfield, W.M. Augustyniak, Physs. Rev. 140 (1965) A202.